Age estimates of isochronous reflection horizons by combining ice core, survey, and synthetic radar data

Olaf Eisen, Uwe Nixdorf, Frank Wilhelms, and Heinrich Miller
Alfred-Wegener-Institut für Polar- und Meeresforschung Bremerhaven, Bremerhaven, Germany

Received 20 October 2003; accepted 26 February 2004; published 20 April 2004.

[1] Ice core records and ice-penetrating radar data contain complementary information on glacial subsurface structure and composition, providing various opportunities for interpreting past and present environmental conditions. To exploit the full range of possible applications, accurate dating of internal radar reflection horizons and knowledge about their constituting features is required. On the basis of three ice core records from Dronning Maud Land, Antarctica, and surface-based radar profiles connecting the drilling locations, we investigate the accuracies involved in transferring age-depth relationships obtained from the ice cores to continuous radar reflections. Two methods are used to date five internal reflection horizons: (1) conventional dating is carried out by converting the travel time of the tracked reflection to a single depth, which is then associated with an age at each core location, and (2) forward modeling of electromagnetic wave propagation is based on dielectric profiling of ice cores and performed to identify the depth ranges from which tracked reflections originate, yielding an age range at each drill site. Statistical analysis of all age estimates results in age uncertainties of 5–10 years for conventional dating and an error range of 1–16 years for forward modeling. For our radar operations at 200 and 250 MHz in the upper 100 m of the ice sheet, comprising some 1000–1500 years of deposition history, final age uncertainties are 8 years in favorable cases and 21 years at the limit of feasibility. About one third of the uncertainty is associated with the initial ice core dating; the remaining part is associated with radar data quality and analysis. *INDEX TERMS:* 0689 Electromagnetics: Wave propagation (4275); 0644 Electromagnetics: Numerical methods; 1827 Hydrology: Glaciology (1863); 1863 Hydrology: Snow and ice (1827); 9310 Information Related to Geographic Region: Antarctica; *KEYWORDS:* ice-penetrating radar, ice core synchronization, synthetic radargrams

Citation: Eisen, O., U. Nixdorf, F. Wilhelms, and H. Miller (2004), Age estimates of isochronous reflection horizons by combining ice core, survey, and synthetic radar data, *J. Geophys. Res.*, *109*, B04106, doi:10.1029/2003JB002858.

1. Introduction

[2] Interpretation of ice cores as paleoclimate archives requires detailed knowledge about their past and present geophysical environment. Different techniques have been developed that facilitate the determination of the present state as well as the reconstruction of past glaciological settings surrounding the drilling locations. The rising number of deep ice cores, being retrieved in Antarctica and Greenland yielding high-quality records, comes along with an increasing demand for improved ice core synchronization, improved numerical ice sheet modeling, and extended surface observations.

[3] Because ice-penetrating radar (IPR) provides a powerful tool to investigate properties of glaciers and ice sheets it is widely used in glaciology. Studies of dielectric properties of ice and internal radar reflection horizons (IRHs) suggest that most processes forming electromagnetic reflectors take place at the glacier surface at approximately the same time. The submergence rate of the isochrone surface is determined by interaction of the flow field and surface accumulation [*Robin et al.*, 1969; *Gudmandsen*, 1975; *Clough*, 1977; *Millar*, 1981; *Bogorodsky et al.*, 1985; *Moore*, 1988]. In general, the reflection of electromagnetic waves occurs where the complex dielectric constant changes. Gradients in the real part, the permittivity, are mostly related to density; they dominate reflections in the upper hundreds of meters. Variations in the imaginary part are proportional to conductivity and related to acidity. They are the governing reflection cause in deeper ice. A third mechanism, proposed by *Harrison* [1973], involves dielectric anisotropy of the crystal fabric. An extensive discussion is given by *Matsuoka et al.* [2003].

[4] IPR has been applied in polar and alpine environments primarily to probe ice thickness in relation to ice core deep drilling projects [e.g., *Hempel and Thyssen*, 1992; *Dahl-Jensen et al.*, 1997; *Steinhage et al.*, 1999; *Nixdorf and Göktaş*, 2001; *Kanagaratma et al.*, 2001]. As a matter of principle, IPR is also used to establish the stratigraphy of IRHs and thus isochronic layers. Such IPR-based mapping of englacial isochrones on a quasi-continuous scale facili-

0148-0227/04/2003JB002858$09.00

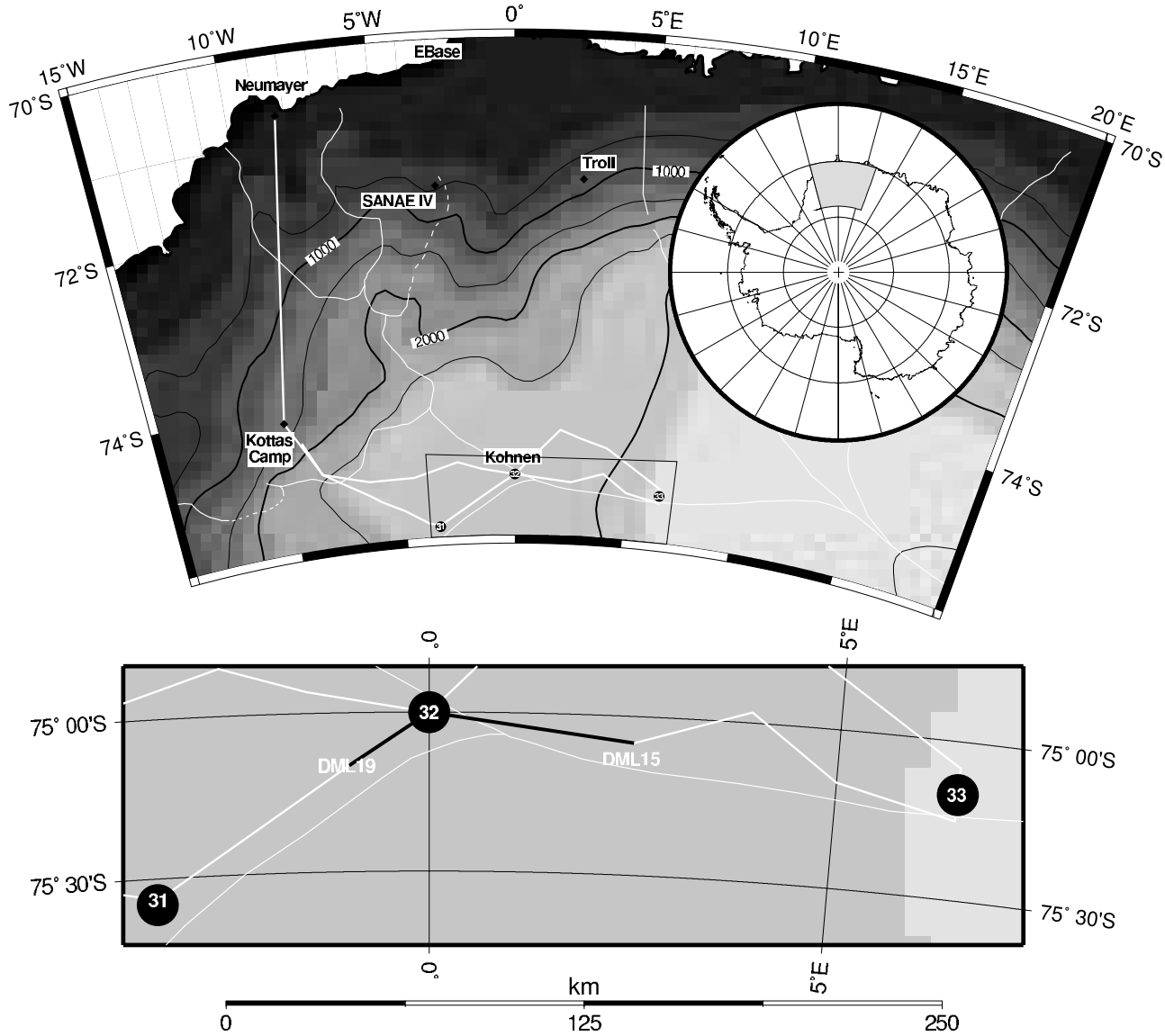

Figure 1. Location map of study area in DML, showing shallow ice core drill sites (B31–B33), summer camps, and research stations. Thick white solid lines are traverse surface-based radar profiles, thin white lines are major ice divides. The top right inset shows the location of DML on the Antarctic continent, the bottom inset indicates the IPR profiles from DML19 (B31) to DML05 (B32) in 2000/2001 and from DML05 to DML15 (B33) in 1998/1999, with the profiles displayed in Figure 3 indicated as black lines.

tates the matching of ice core records [*Jacobel and Hodge*, 1995; *Siegert et al.*, 1998], depiction of vertical strain rates [*Jacobel et al.*, 1993; *Raymond et al.*, 1995; *Hodgkins et al.*, 2000], reconstruction of snow and firn genesis [*Frezzotti et al.*, 2002], determination of spatial distributions of accumulation [*Richardson-Näslund and Holmlund*, 1999; *Nereson and Raymond*, 2001; *Pälli et al.*, 2002], and validation of numerical ice sheet models [*Huybrechts et al.*, 2000; *Baldwin et al.*, 2003].

[5] In this study, our aim is to evaluate the accuracy of age estimates of internal layers. The concept that we use implicitly assumes that the observed IRHs are isochrones. To accomplish our goal we use three dated shallow ice cores from Dronning Maud Land (DML), Antarctica, together with an extensive set of surface-based radar surveys (Figure 1). The combined data set is analyzed by to different methods, namely, conventional dating and numerical forward modeling.

[6] Age-depth profiles, obtained from annual layer counting or wiggle matching of ice core records, are usually transferred to IRHs by mere comparison or correlation techniques in the depth domain. In contrast, radar reflections are recorded as a function of travel time in the so-called time domain. As the radar source signal has a finite length in time, simple travel time-depth conversion results in systematic errors when relating observed reflections to depth. Consequently, this error is also inherent to attributing ages to the IRHs. Although the connection of volcanic events with deeper IRHs might be unambiguous in special cases [*Hempel et al.*, 2000],

Table 1. Properties Derived From Ice Core Data[a]

	B31	B32	B33
General			
Core length, m	115.1	148.9	129.6
Maximum age, years	1536	1885	2142
Accumulation, kg m^{-2} yr^{-1}	62.2	61.1	45.6
DEP Data			
Missing, m	0.84	1.02	0.32
Rejected, m	5.81	7.04	5.82
Total, m	6.65	8.06	6.14

[a]Maximum age from *Sommer et al.* [2000], accumulation averaged from 1259–1997 A.D. [*Oerter et al.*, 2000].

the degree of uncertainty depends in general on geographic location, depth range, and IPR system properties.

[7] Recent advances in forward modeling of radargrams, based on dielectric profiling (DEP) of ice cores, provide a new method to date IRHs. The importance of accurate interpretations of IRHs for these applications has motivated for more than two decades several studies on forward modeling of radar data [e.g., *Moore*, 1988; *Blindow*, 1994; *Miners et al.*, 2002]. In principle, these studies provide the best means to directly investigate reflection mechanisms. The distribution of the dielectric constant with depth can be derived from DEP [*Moore and Paren*, 1987], while the direct current conductivity can be determined from electric conductivity measurements [*Hammer*, 1980]. Because of shortcomings of ice core data and computational resources, earlier forward modeling approaches had limited success. The development of an improved calibrated DEP device for simultaneous measurements of the real and imaginary part of the complex dielectric constant [*Wilhelms*, 2000] provides the basis for recent advances in modeling [*Kohler et al.*, 2003; *Eisen et al.*, 2003a]. By combining high-resolution DEP data with multidimensional finite difference (FD) numerical modeling techniques, *Eisen et al.* [2003b] demonstrated that satisfactory reproduction of surveyed radar data can be achieved. On the basis of their approach and three DEP records, we develop a new method to identify the depth range from which an observed IRH originates and thus to estimate its age.

[8] We first present the utilized ice core and radar data sets and introduce the forward modeling and conventional dating techniques. Second, we apply both methods to estimate the age of five IRHs and examine the errors related to either method. Finally, we join the different data sets and techniques to investigate and answer the main questions, how accurately can we date IRHs?

2. Database

[9] The European Project for Ice Coring in Antarctica (EPICA) aims at retrieving two deep ice cores in different regions of the Antarctic ice sheet. Drilling at Dome Concordia is performed since 1996, the second deep drilling operation started in 2001 at the Kohnen station in DML, near the site DML05 in the Atlantic sector of Antarctica. The study presented here makes use of ice core and radar data obtained during several EPICA presite surveys in DML. The different data sets will be described next.

2.1. Glaciological Settings and Age-Depth Relationships

[10] During the 1997/1998 field season, three shallow ice cores and a number of shallow firn cores were retrieved in DML. With a total length of 115–149 m, the ice cores B31–33 comprise a deposition history of 1536–2142 years (Table 1). The accumulation in DML is in the range of 45–100 kg m^{-2} yr^{-1}, relatively high values for Antarctic conditions [*Oerter et al.*, 2000]. The annual mean temperature is around −45°C, ice thickness at the deep drilling location is estimated to be 2700 m [*Steinhage et al.*, 1999].

[11] Dating of all three ice cores was performed by annual layer counting of multiparameter chemical records in combination with identification of volcanic horizons [*Sommer et al.*, 2000]. In the immediate vicinity of volcanic signals the age-depth relation is accurate to within ±2 years. Between volcanic tie points the resulting age-depth relationship for each ice core has an accuracy between ±5 and ±8 years (Figure 2).

2.2. Ice Core DEP Data

[12] The complex relative dielectric constant of snow and ice can be written as

$$\varepsilon = \varepsilon' - i\varepsilon'' = \varepsilon' - i\frac{\sigma}{\varepsilon_0 \omega} = |\varepsilon| e^{-i\delta}, \quad (1)$$

where the real part ε' is the ordinary relative permittivity and the imaginary part ε'' is the dielectric loss factor of the medium. The latter can be expressed as a function of conductivity σ, angular frequency ω, and the permittivity of vacuum ε_0. The last expression in equation (1) defines the

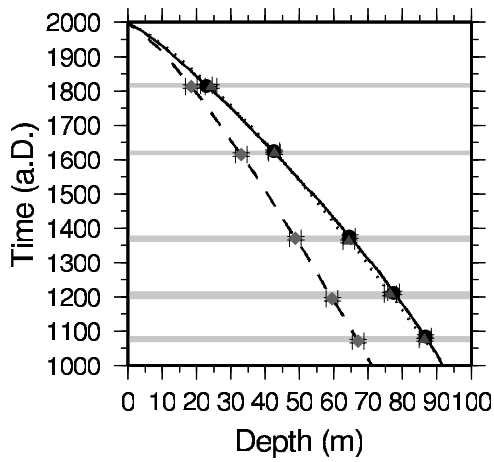

Figure 2. Age-depth relationships for the three shallow ice cores: B31 (solid), B32 (dotted), B33 (dashed) derived from chemical analyses [*Sommer et al.*, 2000]. The symbols represent the age estimates of the five tracked internal reflection horizons at the three boreholes, derived from conventional dating (section 4.1). Vertical error bars are the uncertainty of the ice core dates (5–8 years), horizontal error bars are the theoretical depth errors of the IRH. The horizontal grey bars indicate the range between the oldest and youngest age estimate of each IRH.

loss tangent, where $\tan\delta = \varepsilon''/\varepsilon'$. The electromagnetic wave speed in snow and ice is related to the dielectric constant by

$$c = c_0/\sqrt{\varepsilon}, \quad (2)$$

with c_0 being the electromagnetic wave speed in vacuum.

[13] DEP of the complex ε with a calibrated guarded scanning capacitor and γ-absorption density measurements were performed simultaneously along the 1 m long core sections immediately after retrieval. The combined DEP density device, developed by *Wilhelms et al.* [1998] and improved by *Wilhelms* [2000], operates at a frequency of 250 kHz with an electrode length of 1 cm. Data points were taken in 5 mm increments, providing systematic accuracies for each ε component of 1% and statistical errors of 0.1% after correcting the raw data to an ambient temperature of $-15°C$. A depth error of 1 cm results from the positioning of the core sections in the measuring bench. To identify and correct sections with poor core quality for later analyses, we follow the scheme tested and applied by *Eisen et al.* [2003a]. The running mean and standard deviation of ε' are calculated within a 2.5 m window along the core. DEP values that show a permittivity which is more than one standard deviation below the window mean are rejected, as the lower permittivity values are most likely caused by cracks in the ice. After accounting for data gaps from the drilling operation, the total percentage of missing data for the different cores is around 5% (Table 1).

2.3. Surface-Based Ice-Penetrating Radar

[14] Usually, two types of measurements are performed for radar data acquisition: common midpoint (CMP) and common offset (CO) surveys. The CMP recording technique yields the velocity-depth profile and information about the reflection properties of a single column of small horizontal extent, as the distance between transmitter and receiver is symmetrically increased relative to the stationary center point. For CO surveys, source and receiver are kept at a fixed distance and moved across the surface, providing a picture of the subsurface structure along the survey profile.

[15] We analyze radar measurements from CO measurements between various borehole locations (Figure 1). These measurements were performed with a commercial RAMAC radar set (Malå Geoscience, Sweden). The monopulse bistatic radar system was operated with antennae at 200 and 250 MHz, using unshielded dipoles in a fixed distance of 60 cm in the first case and shielded antennae at a distance of 36 cm in the second case. Both setups are permanently mounted in skid boxes and connected with the central processing unit via fiber optic cables, thus avoiding noise from ohmic conductors. The processing unit was operated by a Husky FC PX5 personal computer, using the radar system software. The 200 MHz survey was carried out in 1999 between B32 and B33, using a snow tractor for pulling at an average speed of 8 km h^{-1}. Traces were recorded every 1.5 m, triggered by a distance wheel, in a 1500 ns time window containing of 2400 samples. The 250 MHz data were recorded in 2001 between B32 and B31, pulling the device by a snow mobile at 12 km h^{-1} with traces recorded every meter in a 1570 ns time window with 2048 samples. For either measurement setup, one stored trace consist of eight stacked pulse recordings.

2.4. Processing and Horizons Tracking

[16] Tracking of coherent patterns in adjacent traces can best be achieved in processed IPR profiles. Processing was performed using Paradigm Geophysical FOCUS version 4.2 software and includes fivefold horizontal stacking, i.e., stacking of adjacent traces along the profile, subsequent bandpass filtering, and automatic gain control with a 50 ns window. IRHs were semiautomatically tracked in the processed data with the Landmark OpenWorks release 2003.0 software. The tracking algorithm exploits the coherency of signal features (e.g., minimum, maximum or zero amplitude) above noise to automatically detect the same feature within a prescribed time window in adjacent traces and follows it as long as a similarity criterion is fulfilled. The tracking process is observed by the user and requires manual interaction in case of a low signal-to-noise ratio. Several IRHs were selected and tracked continuously in the whole region (Figure 3).

3. Forward Modeling of Radargrams

[17] Numerical forward modeling enables the investigation of reflection properties and involved physical processes. Our finite difference time domain model uses the in situ complex dielectric constant and includes wave phenomena occurring during propagation like interferences, an advantage over convolution-type modeling approaches.

3.1. Model Representation of IPR System Characteristics

[18] Different schemes were developed over the decades to employ finite difference (FD) techniques for computational electrodynamics. Whereas several approaches are based on wave equation formulations of only the electric or magnetic field, the algorithm introduced by *Yee* [1966] solves for both electric and magnetic fields in time and space using the coupled Maxwell's curl equations. This provides a robust basis with several advantages over other realizations [*Taflove*, 1995]. We implement the two-dimensional transverse electric version of the Yee algorithm on a staggered grid with leapfrog time integration. The source is an infinite electric line source close to the surface (E_y polarized), and the y component of the electric field E at a preselected position represents the signal recorded by the receiver.

[19] Two sets of IPR parameters are considered for the modeling experiments: the 250 MHz setup at B31 and B32, and the 200 MHz setup at B32 and B33. For each experiment the DEP data are linearly interpolated onto the cartesian space grid, assuming laterally homogeneous values in ice and air, with $\varepsilon_{air} = 1$ and $\sigma_{air} = 0$. Various authors found that the shape of the source wavelet is crucial if observed reflection are to be reproduced by forward modeling [*Moore*, 1988; *Arcone et al.*, 1995; *Hildebrand*, 1996]. To simulate the propagation of the radar wave as close as possible, we use duration and shape of the air waves determined from survey data as the source wavelets (Figure 4) and adopt the IPR source-receiver survey setup geometry for modeling.

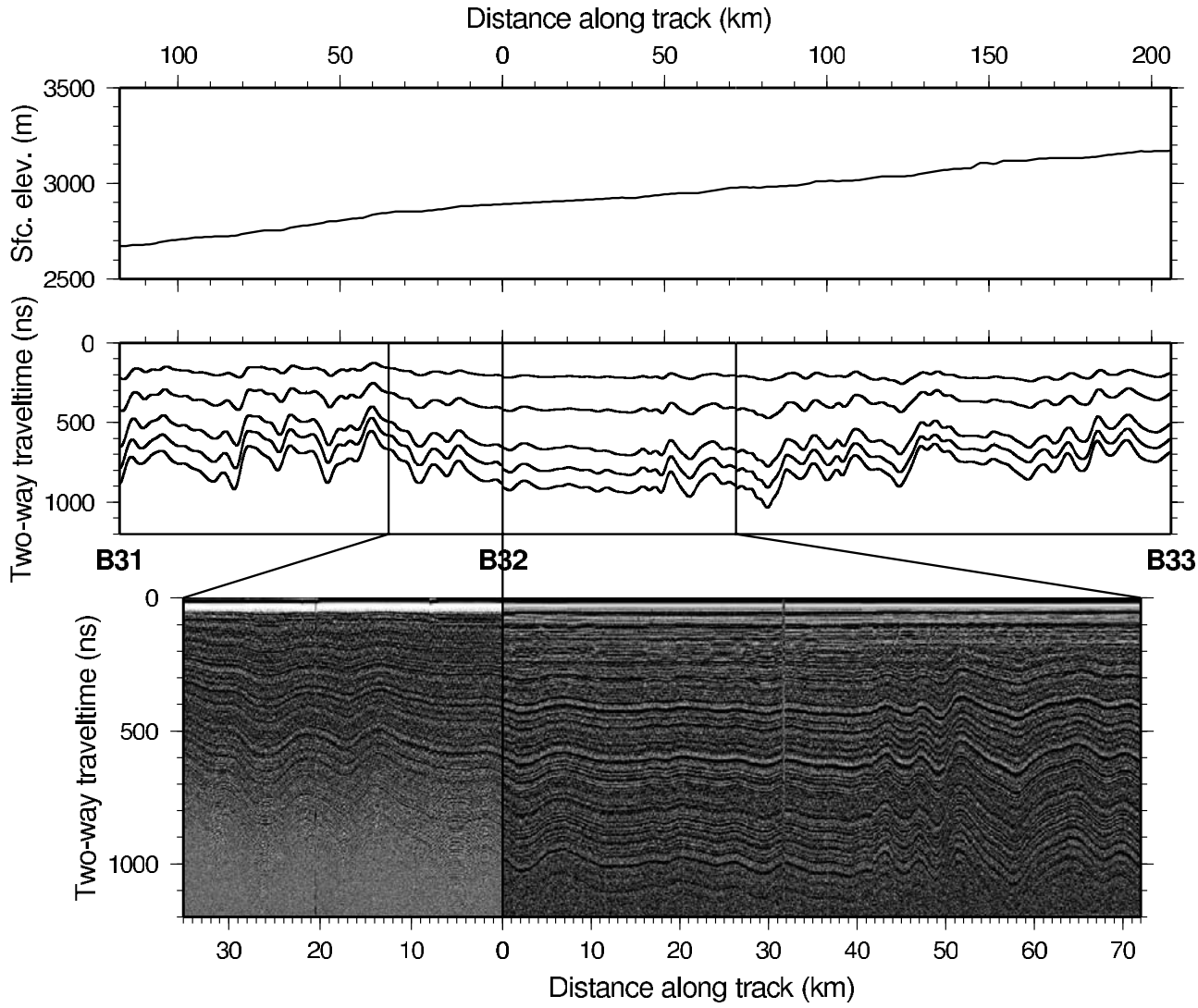

Figure 3. Internal reflections tracked from B31 via B32 to B33 (Figure 1), starting at B32 at two-way travel times (TWTs) of around 210, 420, 650, 780, and 900 ns. (top) Surface elevation along the same profile. (bottom) Two examples of processed common offset profiles are shown, recorded at 250 MHz (B32–B31) and 200 MHz (B32–B33). The grey scale indicates the signal envelope, i.e., magnitude, resulting in an emphasized contrast but lower vertical resolution. Detection limits are around 1000 and 1200 ns for the 250 and 200 MHz signal, respectively. In regions with steeper internal topography, however, signals fade at shallower depths, posing a problem for tracking deeper reflections continuously.

[20] Calculations were performed with a parallelized version of the FD model on a NEC SX-6 supercomputer at the Deutsches Klimarechenzentrum (DKRZ, Hamburg, Germany). Model dimensions for standard runs are 10 m in horizontal and 120 m in vertical direction with an isotropic space increment $\Delta = 0.01$ m and a time increment $\Delta t = 0.01$ ns, thus providing high resolution of the interpolated source pulse (Figure 4), satisfying the Courant stability criterion, and avoiding numerical diffusion [*Taflove*, 1995, pp. 81–106]. Reflections from boundaries of the model domain were reduced by using a 5 m wide absorbing range with exponentially increasing conductivity, thus damping the propagating wave.

3.2. Evaluation of Model Results

[21] Numerical modeling of radargrams provides the opportunity to directly investigate the connection between medium properties and radar observations. Before applying modeling results to in situ problems, the agreement between synthetic and surveyed traces has to be confirmed. Different radar setups, data processing, and display methods were examined to evaluate the agreement between synthetic and surveyed radargrams. These investigations include comparison of single unprocessed traces [*Hildebrand*, 1996; *Miners*, 1998], embedment of synthetic traces in raw CO profiles displayed in variable density representation [*Kohler et al.*, 2003], and comparison of synthetic traces with stacked CO data in wiggle format [*Eisen et al.*, 2003a]. Most successful comparisons were achieved by exploiting the ability of CMP processing to improve the signal-to-noise ratio of measured data [*Eisen et al.*, 2003b].

[22] As the simulation of a three-dimensional wave propagation process with a two-dimensional model is an approximation, a perfect agreement between measured and

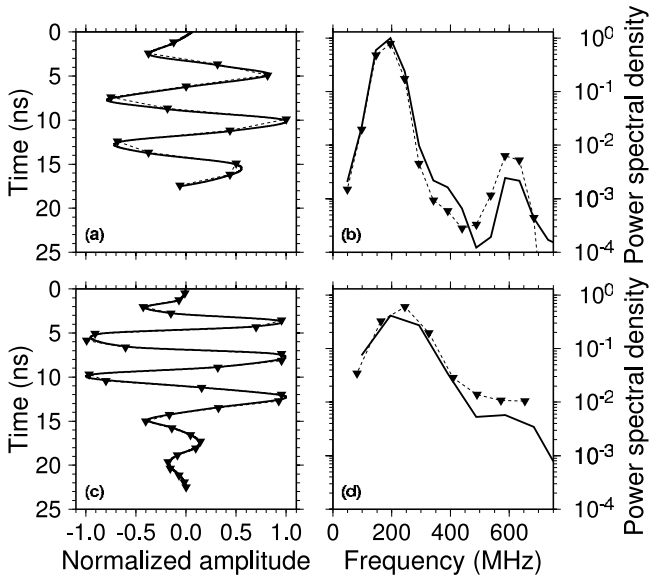

Figure 4. Radar wavelets used for FD modeling: time domain signals of the (a) 200 and (c) 250 MHz antennae and (b) and (d) their corresponding power spectra, respectively. Thin dashed lines with triangles indicate the raw data wavelets taken from the direct air wave, the thick lines denote the Akima spline interpolated resampled wavelets used for modeling.

modeled traces cannot be expected. Especially the falloff of the primary wave amplitude with travel time is different, and thus also the amplitude of reflections. To correct for this difference in amplitude between surveyed and synthetic traces, we apply an automatic gain control for a 100 ns window to both type of traces.

[23] Data from CO surveys at different frequencies and one CMP measurement, all recorded within 100 m of the site B32, are displayed in Figure 5, together with two synthetic traces calculated from DEP data obtained in 1998 at the same site. The traces displayed in Figures 5a–5c were recorded in 1999 with the 200 MHz CO setup, each consisting of 30 stacks of the raw radar recordings. A normal moveout corrected and stacked CMP measurement from the same year is shown in Figure 5d. It is clearly visible that the background noise in Figure 5d is lower than in the CO-based traces in Figures 5a–5c. Only major reflections are clearly visible in all four traces. The synthetic radargram in Figure 5e is based on 200 MHz system characteristics (Figure 4a). The noise content is comparable to the one present in the CO data, the amplitude of reproduced reflections in Figure 5e is, in general, different from the ones in Figures 5a–5d. The traces in Figures 5f and 5g are 30-fold stacked CO data recorded at 250 MHz in 1999 and 2001, respectively. Here, again, only major reflections have the same characteristics. The synthetic trace in Figure 5h is based on the 250 MHz system characteristics (Figure 4c). Although major reflections are reproduced, detailed characteristics in phase and amplitude differ.

[24] All eight traces compared in Figure 5 depend on the dielectric properties of the same column of ice. It is evident that the small-scale spatial and temporal variability of physical properties of firn over a distance of less than 100 m and a time span of 4 a imposes the most severe problem on the objective reproducibility. Horizontal stacking of radar data to reduce noise can only partly improve the effect of lateral inhomogeneities, the utilization of dielectric properties of only one core for forward modeling of synthetic radargrams does not account for this influence (L. Karlöf, personal communication, 2002).

[25] Despite the better agreement of CMP data with synthetic traces (see Figures 5d and 5e for B32) the goals in this study require to achieve sufficient reproducibility of CO traces of interest by synthetic radargrams to associate continuous IRHs with dielectric properties in the ice core records. To this end we perform comparisons of synthetic radargrams with corresponding CO traces at each drilling location. Two comparisons are carried out with the 250 MHz CO data at B31 and B32, and another two for

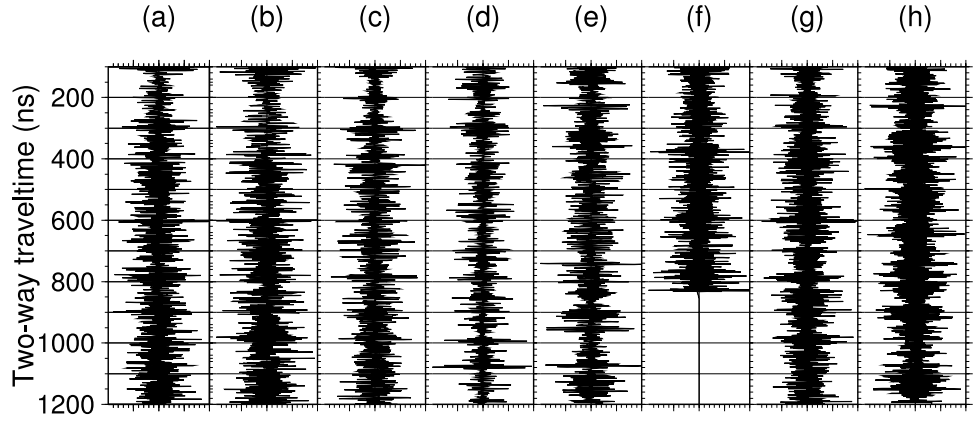

Figure 5. Single trace comparison of different data sets from B32, demonstrating the difficulty to reproduce individual reflection characteristics. (a)–(c) Traces from 30-fold stacked 200 MHz CO data, (d) derived from a normal moveout-corrected CMP survey. (f) and (g) CO data from different years, recorded at 250 MHz and also processed with 30-fold horizontal stacking. (e) and (h) Synthetic radar traces, representing 200 and 250 MHz experiments, respectively. Automatic gain control has been applied to 100 ns windows.

Table 2. Dating of IRHs at Borehole Locations[a]

Ice Core	210 ns	415 ns	650 ns	780 ns	890 ns
			Conventional Dating		
B31	1815	1624	1376	1212	1085
B32	1822	1619	1362	1208	1075
B33	1813	1615	1371	1194	1071
Mean	1817	1619	1370	1205	1077
SD	±5	±5	±7	±10	±7
			FD Sensitivity Studies		
B31	1819–1809	1645–1632	1394–1382	1233–1215	1097–1081
B32	1819–1807	1645–1627	1374–1360	1229–1210	1092–1078
B33	1820–1808	1647–1633	1395–1364	1213–1185	1093–1067
Mean	1819–1808	1646–1631	1388–1369	1225–1204	1094–1075
SD	±1 ±1	±1 ±3	±12 ±12	±11 ±16	±3 ±7

[a]IRHs are identified by their travel time at B32, all dates are given in years A.D., and the errors are given in years. Age-depth relationships for each core are taken from *Sommer et al.* [2000], rounded to whole years and accurate to 5–8 years. The listed errors are the standard deviations (SD) in respect to the three age estimates of each IRH.

the 200 MHz data at B32 and B33. At least five reflections can be identified that are continuous in the CO profiles between all three drilling locations and are at the same time reproduced to a sufficient degree of accuracy by all four modeling experiments with the corresponding ice core records. The analyses described in section 4 will focus on the age estimates of these tracked IRHs.

4. Analyses and Interpretations

[26] To evaluate the accuracy of IRH age estimates, we, first, apply conventional dating to the combined ice core and radar data sets and, second, perform numerical sensitivity studies to identify the depth range of origin of the IRHs.

4.1. Conventional Dating of IRHs

[27] Usually, radar data are recorded in the time domain, i.e., reflection amplitude and phase as a function of travel time. To associate ice core profiles and radar data, the latter have to be converted to the depth domain. Most precise travel time-depth functions can be obtained from integration of the DEP-based wave speed (equation (2)), accurate to within 1% [*Eisen et al.*, 2002]. After conversion, each signal in the radargram is associated with a specific depth. This allows to associate each tracked horizon with the age that is available from age-depth relationships at ice core locations in the corresponding depths. Performing these travel time-depth-age conversions at all three drill sites yields three age estimates for each tracked IRH (conventional dating in Table 2). The standard deviation of the mean age of the tracked signals varies between 5 and 10 years, the total standard deviation derived from all values results as 7 years. Although these statistical errors are a reasonable first guess for the accuracy of the age estimates, several additional errors have to be accounted for.

[28] Theoretically, tracking of individual phases of an IRH is accurate to within $\lambda/4$, where λ is the wavelength of the electromagnetic wave. However, this value can be achieved only if the data are recorded at a high sampling rate, which is, in general, a trade-off against long recording windows. Although system settings during our radar surveys fulfill requirements to reach this accuracy, measurement noise and lateral variations of the reflection properties do not allow tracking of coherent signals to this limit. For low noise content, the continuous tracking of an individual phase can be as accurate as $\pm\lambda/2$, that is ±0.5 m or 2.5 ns for the 200 MHz data in firn (assuming a velocity in firn of $c_{\mathrm{firn}} = 2 \times 10^8$ m s^{-1}). In respect to the ice core dates, this corresponds to an age error of ±6.5 years at B31 and B32, and ±8.5 years at B33 below 40 m depth, with slightly lower values above. If the reflector is faint, or if the internal structure is subject to strong undulations in depth, continuous tracking of a individual phase might not be possible. Nevertheless, the reflector itself might still be continuous and trackable at a lower accuracy, limited by the length of the energetic part of the source wavelet, which is around 10 ns in our case (Figure 4). Tracking of these low-quality reflections is then accurate to within ~5 ns (1 m), corresponding to an age uncertainty of approximately 13 years at B31 and B32 and 17 years at B33. Errors derived from this theoretical analysis are about twice as large as the standard deviations calculated from comparison at the three drill sites above (Table 2). This implies that standard deviations are well within the theoretically reliable range.

[29] The finite length of the source signal leads to an additional systematic error. As the individual phases of the source signal (Figure 4) are reflected at slightly different depth levels at the same time, interference takes place. This results in an uneven distribution of reflected energy among the individual phases of the source wavelet. The IRH-tracking procedure described above (section 2.4) follows a coherent amplitude feature within a dominant horizon, which usually corresponds to a single phase within the received signal. Tracking this feature therefore might lead to an error in absolute travel time as the zero point is defined in respect to the first arrival of the source signal at the receiver. Consequently, the depth of the tracked feature might be subject to an offset in respect to the zero point of the depth scale, and thus also age. From analysis of the shape of the reflection signals we estimate the maximum offset error to be one cycle if the IRH consists of several strong phases, about twice as large as the tracking error derived above. If only one phase is present, it can be neglected.

[30] Conventional age estimates IRHs and subsequent feature tracking finally yield a single age estimate for each reflection horizon. The combination of all error sources (uncertainty in phase selection, tracking, and age-depth

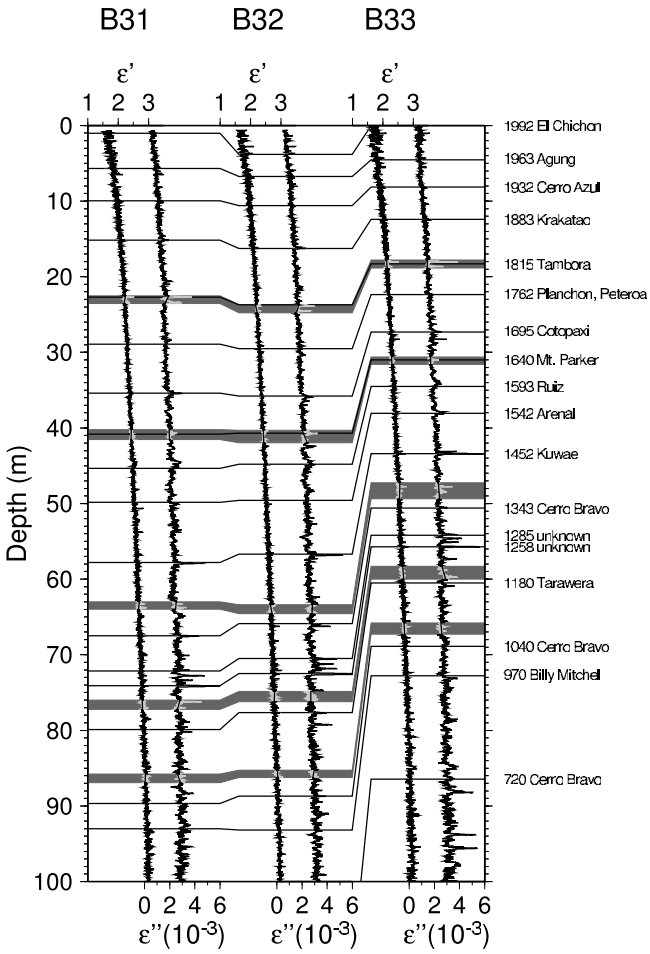

Figure 6. Pairs of measured (left) ordinary relative permittivity ε' and (right) dielectric loss factor ε'' as a function of depth of the ice cores B31, B32, and B33. Selected volcanic events are indicated on the right; their depths at the different locations are indicated by the thin solid lines. Dating is taken from *Sommer et al.* [2000]; volcanic events at B32 are from *Göktaş* [2002]. The grey shaded bars indicate the depth sections for which DEP values are removed and linearly interpolated for sensitivity studies. Within the bars, original data are shown in light grey, interpolate data in black.

relation) for a best case scenario, continuous tracking of single phases and highly accurate ice core ages, is on the order of 8 years. The worst case, highly variable but still continuous reflectors consisting of several phases, lower accuracy of the age-depth relation, yields an error of about 21 years.

4.2. IRH Age Estimates by Forward Modeling

[31] From a simplistic information theory point of view, forward modeling encodes and transforms the information contained in the ε-depth distribution to the time domain format of a radargram. We now use this relation between ice core DEP data and synthetic radargrams to identify depth sections from which the tracked IRHs originate. Associating the age range of these depth sections with the corresponding IRHs then yields a second set of age estimates for each horizon. A number of FD sensitivity runs are carried out to this end.

[32] In each sensitivity run, DEP data in the vicinity of the depth that approximately corresponds to the travel time of an IRH at a drill site are removed. The data gap is then replaced by linear interpolation. As the dielectric gradients in the interpolated sections are smoother than in the original data, forward modeling computations will results in reflection distributions that are different from the original ones. Ideally, the reflections of interest should completely vanish in the sensitivity runs. At the same time, least DEP data as possible should be interpolated to remove a reflection. As this cannot be expected a priori, the identification of depth sections responsible for IRHs is an iterative process carried out manually.

[33] The final results demonstrate that forward modeling indeed enables the association of DEP sections and reflections. The DEP sections of all three ice cores identified to be responsible for the five tracked IRHs by the sensitivity runs are marked by the shaded horizontal bars in Figure 6. Their influence on the synthetic radargrams becomes evident by comparing the runs calculated from the original and interpolated DEP data (Figure 7). Strong reflections in the original synthetic radargram are much weaker, and partly even vanish, in the radargrams calculated from interpolated DEP section.

[34] For each IRH, there is not just one depth available at a borehole location, but a depth range from which it originates. The corresponding age range can be associated with the IRH (Table 2). The errors involved in estimating the age of an IRH tracked between ice core sites are different than the ones analyzed above for conventional dating. As long as it is possible to track a distinct reflector, loosing of phases during tracking is not as significant, as the onset and end in travel time and depth of the reflector are available at each drilling location. Likewise, as the finite length of the source signal is taken into account for modeling, it does not contribute to the total error estimates.

[35] In contrast, the interference of adjacent reflectors still requires the continuity of phases for reliable age estimates. The theoretical estimates for conventional dating presented above do rely on the assumption that a single feature in ε causes the reflection. If several strong ε features occur over a short vertical distance, the travel time from one reflecting feature to the next could be less than the length of the source wavelet. The individually reflected wave trains then superimpose, leading to interference patterns. The recorded reflections may be difficult to separate in the surveyed radar profile, but the different depth (respective age) ranges of origin can still be identified by forward modeling.

[36] Despite of these advantages over conventional dating of isochrones, there are several other factors that determine the quality of age estimates by FD sensitivity studies: (1) the reproducibility of the surveyed reflections by DEP-based forward modeling in comparison to the measured radargram; (2) the quality and resolution of the measured radar data; and (3) the strength of the reflections under consideration. The first factor depends on the quality of the DEP data, as lacking ice core data result in synthetic radargrams of poorer agreement with the mea-

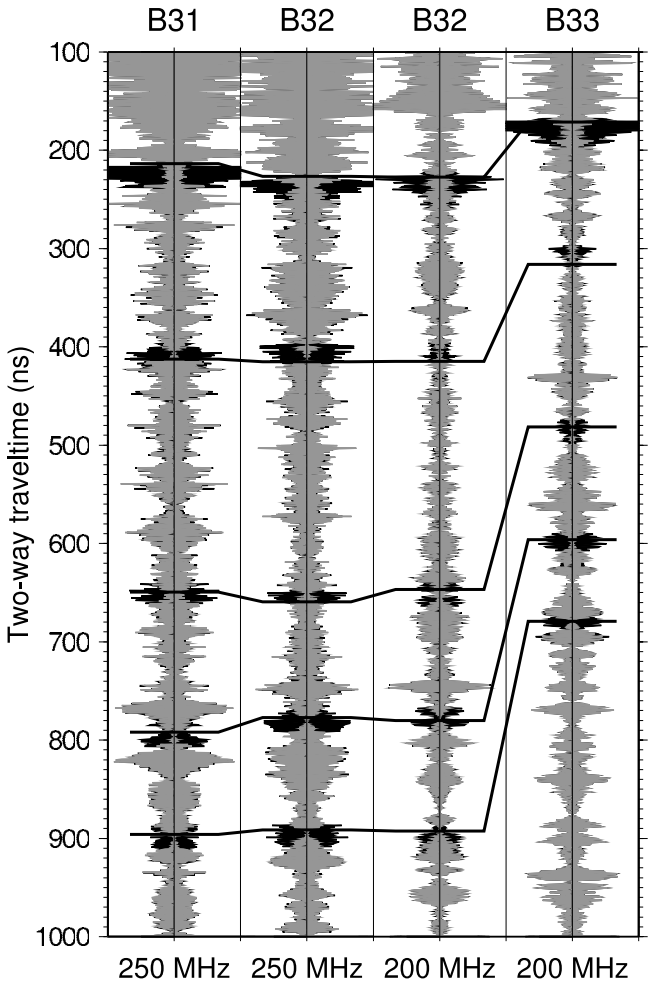

Figure 7. Results of IRH sensitivity studies at B31, B32, B33 with 250 and 200 MHz. The original synthetic radargrams are plotted in black; the results of the sensitivity studies are plotted in grey on top. In both cases the signal envelope is displayed as positive and negative values to increase clarity. The reflections appearing in black are missing in the sensitivity results because of removed DEP data (Figure 6). The horizontal step-like black lines indicate the depth of the tracked IRHs at each location.

sured trace. Likewise, approximations inherent to the FD approach might cause differences between synthetic and surveyed radargrams. The radar system and data characteristics (geometry, wave properties, processing) and their representation in the FD model are important for the second point. Reflection properties, for instance, strongly depend on the source wavelet (e.g., compare the reflection characteristic at 790 ns at B32 for 200 and 250 MHz in Figure 7). Usage of the wrong wavelet for modeling results in different amplitudes and phases. The third factor obviously depends on the signal-to-noise ratio of a horizon, as a lower ratio decreases accuracies with which individual reflections can be identified (e.g., the 200 MHz reflections at 650 and 480 ns at B32 and B31, respectively).

[37] The statistical analyses of age range estimates yield errors that show a larger scatter than the standard deviations calculated from the conventional dating approach. Depending on the reflector, they range from ±1 years (IRHs at 210 and 415 ns at B32) to ±12 years, and in one case even 16 years (IRH at 780 ns at B32) (Table 2). For the same IRHs, the conventional dating yields age errors between 5 and 10 years. The averaged standard deviations, derived separately from the two individual sets of age estimates, are almost identical. It is just slightly larger for the FD sensitivity studies (8 years) than the one obtained earlier from conventional dating (7 years). This accentuates the validity of both error estimates.

5. Summary and Outlook

[38] A common problem in ice core interpretation is the different quality of age scales, derived from various techniques. Our results emphasize the complementary character of ice core records and radar data. Whereas the first is one-dimensional and highly accurate in depth, the second is two-dimensional with reduced depth accuracy. Merging ice core data, radar data, and different analysis methods on larger horizontal and vertical scales helps to remedy ambiguities in glaciological interpretations.

[39] In this study we estimated the age of five reflection horizons that were tracked between three shallow ice core locations by two different methods. Conventional dating was carried out by mere comparison of IRH depths with ice core age-depth relations and implies an instantaneous age for each IRH. Forward modeling, on the other hand, identified the depth sections in the ice core record which cause the IRHs. As each depth section corresponds to an age range, it is questioned whether the concept of an instantaneous age for an IRH is correct.

[40] Tracking IRHs between three shallow ice cores provides the basis for a sound statistical error analysis of age estimates. The average errors are comparable in both methods, being around 7–8 years. The relative error is around 1–3%, depending on the age of the reflector. If individual reflectors can be accurately reproduced by synthetic radargrams, forward modeling even yields an age error of 1 year, less than 0.5% of the reflector age. On the other hand, if a good agreement between measured and modeled trace is not achieved or a reflector cannot be clearly distinguished in the synthetic radargram, the error made by only using forward modeling could be almost twice as large as if conventional dating was used. In any case, the data-based statistical errors are well within the theoretical limits. This proofs that the initial assumption, i.e., that the considered IRHs are isochrones, was indeed justified.

[41] The accuracy of the age estimates encourages several applications involving radar data, e.g., extrapolation and synchronization of ice core properties. While radar characteristics seem to define the upper bound for age estimates in the upper part of the ice sheet, the large increase of the age rate with depth is the limiting factor for highly accurate estimates of reflector ages in the deeper regions. Although sensitivity studies with FD forward modeling are a time-consuming trial-and-error scheme, we expect that the accuracy of age estimates could be significantly increased for deeper layers. As they can reveal the depth range of origin of reflections the larger effort is worth while. The ultimate

goal, of course, is the direct accurate inversion of radar data to yield DEP distributions as a two-dimensional profile, a goal that still requires strong efforts for several years.

[42] In this context, the methods presented here also promise useful application for analyses of remaining problems in deeper parts of the Greenlandic and Antarctic ice sheets, e.g., the connection of all deep drilling sites by ice penetrating radar and synchronization of ice core records independently of isotopes or gases. This study is a first step, as results are unambiguous in upper layers, but will become even more important if the technique is extended to deeper regions of the ice sheet where several physical processes leading to reflections of comparable magnitude show up. Namely, the contribution of fabric orientations and rapid changes therein to the electromagnetic reflectivity can be investigated in further detail when high-resolution DEP profiles and corresponding radar surveys of several ice cores are available. These data sets should be obtained in the next few years from the EPICA and other deep ice cores.

[43] **Acknowledgments.** The original version of the FDTD model was developed by Volker Mayer and Jupp Sandmeier as a module for the commercial radar and seismic analysis PC software Reflex (Sandmeier Software, Karlsruhe, Germany). They gave helpful advice for decoupling the module from the PC software for our special purposes. Debugging and optimization greatly profited from support by Stephan Frickenhaus, AWI computing centre, and Klaus Ketelsen, DKRZ. Preparation of this work was supported by the Deutsche Forschungsgemeinschaft grant Ni493/1 and two scholarships of the Studienstiftung des Deutschen Volkes. This work is a contribution to the European Project for Ice Coring in Antarctica (EPICA), a joint ESF (European Science Foundation)/EC scientific programme, funded by the European Commission and by national contributions from Belgium, Denmark, France, Germany, Italy, Netherlands, Norway, Sweden, Switzerland, and United Kingdom. This is EPICA publication 95.

References

Arcone, S., D. Lawson, and A. Delaney (1995), Short-pulse wavelet recovery and resolution of dielectric contrasts within englacial and basal ice of Matanuska Glacier, Alaska, U.S.A., *J. Glaciol.*, *41*, 68–86.

Baldwin, D. J., J. L. Bamber, A. J. Payne, and R. L. Layberry (2003), Using internal layers from the Greenland Ice Sheet, identified from radio-echo sounding data, with numerical models, *Ann. Glaciol.*, *37*, 325–330.

Blindow, N. (1994), Reflection amplitudes of 40 MHz monopulse radio echo sounding: Correlation with ice core data and ice dynamics, *Filchner-Ronne Ice Shelf Programme Rep. 8*, pp. 5–8, Alfred Wegener Inst. for Polar and Mar. Res. Bremerhaven, Bremerhaven, Germany.

Bogorodsky, V., C. Bentley, and P. Gudmandsen (1985), *Radioglaciology*, D. Reidel, Norwell, Mass.

Clough, J. W. (1977), Radio echo sounding: Reflections from internal layers in ice sheets, *J. Glaciol.*, *18*, 3–14.

Dahl-Jensen, D., et al. (1997), A search in North Greenland for a new ice-core drill site, *J. Glaciol.*, *43*, 300–306.

Eisen, O., U. Nixdorf, F. Wilhelms, and H. Miller (2002), Electromagnetic wave speed in polar ice: Validation of the CMP technique with high resolution DEP and γ-density measurements, *Ann. Glaciol.*, *34*, 150–156.

Eisen, O., F. Wilhelms, U. Nixdorf, and H. Miller (2003a), Identifying isochrones in GPR profiles from DEP-based forward modelling, *Ann. Glaciol.*, *37*, 344–350.

Eisen, O., F. Wilhelms, U. Nixdorf, and H. Miller (2003b), Revealing the nature of radar reflections in ice: DEP-based FDTD forward modeling, *Geophys. Res. Lett.*, *30*(5), 1218, doi:10.1029/2002GL016403.

Frezzotti, M., S. Gandolfi, and S. Urbini (2002), Snow megadunes in Antarctica: Sedimentary structure and genesis, *J. Geophys. Res.*, *107*(D18), 4344, doi:10.1029/2001JD000673.

Göktaş, F. (2002), Characterisation of glacio-chemical and glacio-meteorological parameters of Amundsenisen, Dronning Maud Land, Antarctica, *Ber. Polarforschung 425*, Alfred-Wegener-Inst. für Polar- und Meeresforsch., Bremerhaven, Germany.

Gudmandsen, P. (1975), Layer echoes in polar ice sheets, *J. Glaciol.*, *15*, 95–101.

Hammer, C. (1980), Acidity of polar ice cores in relation to absolute dating, past volcanism, and radio-echoes, *J. Glaciol.*, *25*, 359–372.

Harrison, C. H. (1973), Radio echo sounding of horizontal layers in ice, *J. Glaciol.*, *12*, 383–397.

Hempel, L., and F. Thyssen (1992), Deep Radio Echo Soundings in the vicinity of GRIP and GISP2 Drill Sites, Greenland, *Polarforschung*, *62*, 11–16.

Hempel, L., F. Thyssen, N. Gundestrup, H. B. Clausen, and H. Miller (2000), A comparison of radio-echo sounding data and electrical conductivity of the GRIP ice core, *J. Glaciol.*, *46*, 369–374.

Hildebrand, A. (1996), Untersuchung der Laufzeit- und Amplitudenverhalten elektromagnetischer Impulse bei glaziologischen Radarmessungen, Ph.D. thesis, Westfälische Wilhelmsuniv. Münster, Münster, Germany.

Hodgkins, R., M. J. Siegert, and J. A. Dowdeswell (2000), Geophysical investigations of ice-sheet internal layering and deformation in the Dome C region of central East Antarctica, *J. Glaciol.*, *46*, 161–166.

Huybrechts, P., D. Steinhage, F. Wilhelms, and J. Bamber (2000), Balance velocities and measured properties of the Antarctic ice sheet from a new compilation of gridded data for modeling, *Ann. Glaciol.*, *30*, 52–60.

Jacobel, R., and S. Hodge (1995), Radar internal layers from the Greenland summit, *Geophys. Res. Lett.*, *22*, 587–590.

Jacobel, R. W., A. M. Gades, D. L. Gottschling, S. M. Hodge, and D. L. Wright (1993), Interpretation of radar-detected internal layer folding in West Antarctic ice streams, *J. Glaciol.*, *39*, 528–537.

Kanagaratma, P., S. P. Gogineni, N. Gundestrup, and L. Larsen (2001), High-resolution radar mapping of internal layers at the North Greenland Ice Core Project, *J. Geophys. Res.*, *106*, 33,799–33,811.

Kohler, J., J. C. Moore, and E. Isaksson (2003), Comparison of modelled and observed responses of a glacier snowpack to ground-penetrating radar, *Ann. Glaciol.*, *37*, 293–297.

Matsuoka, K., T. Furukawa, S. Fujita, H. Maeno, S. Uratsuka, R. Naruse, and O. Watanabe (2003), Crystal orientation fabrics within the Antarctic ice sheet revealed by a multipolarization plane and dual-frequency radar survey, *J. Geophys. Res.*, *108*(B10), 2499, doi:10.1029/2003JB002425.

Millar, D. H. H. (1981), Radio echo layering in polar ice sheets and past volcanic activity, *Nature*, *292*, 441–443.

Miners, W. D. (1998), Electromagnetic reflections inside ice sheets, Ph.D. thesis, Open Univ., London.

Miners, W. D., E. W. Wolff, J. C. Moore, R. Jacobel, and L. Hempel (2002), Modeling the radio echo reflections inside the ice sheet at Summit, Greenland, *J. Geophys. Res.*, *107*(B8), 2172, doi:10.1029/2001JB000535.

Moore, J. (1988), Dielectric variability of a 130 m Antarctic ice core: Implications for radar sounding, *Ann. Glaciol.*, *11*, 95–99.

Moore, J., and J. Paren (1987), New technique for dielectric logging of Antarctic ice cores, *J. Phys. Colloq. C1*, *48*, 155–160.

Nereson, N. A., and C. F. Raymond (2001), The elevation history of ice streams and the spatial accumulation pattern along the Siple Coast of West Antarctica inferred from ground-based radar data from three inter-ice-stream ridges, *J. Glaciol.*, *47*, 303–313.

Nixdorf, U., and F. Göktaş (2001), Spatial depth distribution of the subglacial bed and internal layers in the ice around NGRIP, Greenland, derived with airborne RES, *J. Appl. Geophys.*, *47*, 175–182.

Oerter, H., F. Wilhelms, F. Jung-Rothenhäusler, F. Göktaş, H. Miller, W. Graf, and S. Sommer (2000), Accumulation rates in Dronning Maud Land as revealed by dielectrical-profiling measurements at shallow firn cores, *Ann. Glaciol.*, *30*, 27–34.

Pälli, A., J. C. Kohler, E. Isaksson, J. C. Moore, J. F. Pinglot, V. A. Pohjola, and H. Samuelsson (2002), Spatial and temporal variability of snow accumulation using ground-penetrating radar and ice cores on a Svalbard glacier, *J. Glaciol.*, *48*, 417–424.

Raymond, C. F., N. Nereson, A. M. Gades, H. Conway, R. Jacobel, and T. Scambos (1995), Geometry and stratigraphy of Siple Dome, Antarctica, *Antarct. J. U.S.*, *30*, 91–93.

Richardson-Näslund, C., and P. Holmlund (1999), Spatial variablility in shallow snow-layer depths in central Dronning Maud Land, East Antarctica, *Ann. Glaciol.*, *29*, 10–16.

Robin, G. d. Q., S. Evans, and J. T. Bailey (1969), Interpretation of radio echo sounding in polar ice sheets, *Philos. Trans. R. Soc. London, Ser. A, 146*, 437–505.

Siegert, M. J., R. Hodgkins, and J. A. Dowdeswell (1998), A chronology for the Dome C deep ice-core site through radio-echo layer correlation with the Vostok ice core, Antarctica, *Geophys. Res. Lett.*, *25*, 1019–1022.

Sommer, S., et al. (2000), Glacio-chemical study covering the past 2 kyr on three ice cores from Dronning Maud Land, Antarctica: 1. Annually resolved accumulation rates, *J. Geophys. Res.*, *105*, 29,411–29,421.

Steinhage, D., U. Nixdorf, U. Meyer, and H. Miller (1999), New maps of the ice thickness and subglacial topography in Dronning Maud Land, Antarctica, determined by means of airborne radio echo sounding, *Ann. Glaciol.*, *29*, 267–272.

Taflove, A. (1995), *Computational Electrodynamics: The Finite-Difference Time-Domain Method*, Artech House, Norwood, Mass.

Wilhelms, F. (2000), Measurement of dielectric properties of polar ice cores (in German), *Ber. Polarforschung 367*, Alfred-Wegener-Inst. für Polar- und Meeresforsch., Bremerhaven, Germany.

Wilhelms, F., J. Kipfstuhl, H. Miller, K. Heinloth, and J. Firestone (1998), Precise dielectric profiling of ice cores: a new device with improved guarding and its theory, *J. Glaciol.*, *44*, 171–174.

Yee, K. S. (1966), Numerical solution of initial boundary value problems involving Maxwell's equations in isotropic media, *IEEE Trans. Antennas Propagat.*, *14*, 302–307.

O. Eisen, H. Miller, U. Nixdorf, and F. Wilhelms, Alfred-Wegener-Institut für Polar- und Meeresforschung, Postfach 120161, D-27515 Bremerhaven, Germany. (oeisen@awi-bremerhaven.de)